processes

MDPI

*Article*

# Aluminum-Free Steelmaking: Desulfurization and Nonmetallic Inclusion Evolution of Si-Killed Steel in Contact with $CaO-SiO_2-CaF_2-MgO$ Slag

**Stephano P. T. Piva and Petrus Christiaan Pistorius ***

Department of Materials Science and Engineering, Carnegie Mellon University, Pittsburgh, PA 15213, USA; stephanopiva@gmail.com

* Correspondence: pistorius@cmu.edu

**Abstract:** In some applications, deep desulfurization and deoxidation of steels without the use of aluminum are required, using Si as a deoxidant instead, with double-saturated slags in the $CaO-SiO_2-CaF_2-MgO$ system. This work studied the desulfurization and nonmetallic inclusion evolution for the system using an induction furnace and compared the results with FactSage kinetic simulations. Steel samples were taken from the steel melt and analyzed with ICP-MS and combustion analysis for chemistry, and SEM/EDS for nonmetallic inclusion quantity, size, and composition. The results indicate that the steel was deeply desulfurized, with a final sulfur partition coefficient of 580; MgO was reduced from the slag, yielding dissolved [Mg] that transformed liquid Mn–silicate inclusions into forsterite and MgO. Intentional reoxidation of the melt with oxidized electrolytic iron demonstrated a significant concentration of dissolved [Mg] in the steel, by the formation of additional forsterite and MgO upon reoxidation.

**Keywords:** steelmaking; slag; kinetics; clean steel; nonmetallic inclusions; ladle treatment



**Citation:** Piva, S.P.T.; Pistorius, P.C. Aluminum-Free Steelmaking: Desulfurization and Nonmetallic Inclusion Evolution of Si-Killed Steel in Contact with $CaO-SiO_2-CaF_2-MgO$ Slag. *Processes* **2021**, *9*, 1258. https://doi.org/10.3390/pr9081258

Academic Editors: Chenn Q. Zhou and Tyamo Okosun

Received: 15 June 2021
Accepted: 16 July 2021
Published: 21 July 2021



## 1. Introduction

For certain steel products, alumina-containing nonmetallic inclusions are undesirable, whether because of their effect on steel castability (the tendency of solid alumina and spinel inclusions to clog nozzles) or on product quality (due to the hardness and high melting point of alumina-based inclusions). In certain applications, deformable, liquid inclusions such as manganese silicates are more desirable [1]. Manganese sulfides can impair product toughness, and their formation is limited by decreasing the concentration of sulfur in the liquid steel. To avoid aluminum pickup and enable deep desulfurization, slags in the $CaO-SiO_2-CaF_2-MgO$ system are typically used in such cases: fluorspar ($CaF_2$) significantly increases the solubility of CaO [2], while the absence of $Al_2O_3$ avoids aluminum pickup.

To obtain the deep levels of deoxidation and desulfurization (often obtained by the addition of aluminum as a deoxidant), many processes instead rely on silicon as a primary deoxidant. To obtain a low oxygen activity at the steel–slag interface, to enable deep desulfurization, the silica activity in the slag must be low when using Si as deoxidant. The basic nature of CaO-rich, $CaF_2$-bearing slags and the high solubility of CaO allow liquid slags with low silica activity to be used. The low silica activity (deeply reducing conditions) also drives the reduction of other oxides such as MgO and CaO from the slag, yielding dissolved magnesium and calcium [Mg] and [Ca] in the steel. Reduction of MgO from slag, refractory, or both has been demonstrated for both Si-killed and Al-killed steel types [3–5]. The resulting [Mg] can react with nonmetallic inclusions in steel, for example, transforming alumina inclusions into spinels and periclase (in Al-killed steel). The reduction of CaO does not seem to significantly affect nonmetallic inclusions in most cases, because the near-zero solubility of Ca in steel (at typical secondary-metallurgy oxygen activities) limits the rate of Ca transfer from slag to steel [6,7].

If $Al_2O_3$ were present in such slags, the alumina would likewise be reduced readily; the resulting [Al] would react with liquid manganese silicates (deoxidation products) in the steel, forming potentially solid alumina-containing phases. Although the transient inclusion pathway for steels in contact with $Al_2O_3$-bearing slag is well known [4,8,9], the inclusion pathway for Si-killed steels in contact with slags in the CaO-$SiO_2$-$CaF_2$-MgO system has not been described in the literature.

The industrial approach to using fluoride-based slag to desulfurize Si-killed steel has been well described [10,11]. However, fundamental laboratory studies of this approach have not been reported, and until recently, thermodynamic modeling of the reactions was not feasible because of the paucity of relevant thermodynamic data. Recent updates to commercial thermodynamic packages such as Thermo-Calc [12] and FactSage [13] have added solution models for slags containing significant concentrations of $CaF_2$, enabling thermodynamic and kinetic modeling of the reaction of steel with fluoride-containing slag.

In the work reported here, changes in oxide inclusion composition during desulfurization and concomitant MgO reduction from $Al_2O_3$-free slags were experimentally characterized and compared with thermodynamic and kinetic modeling.

## 2. Materials and Methods

### *2.1. Experimental Setup*

Secondary steelmaking refining was simulated on laboratory scale by using a high-frequency induction furnace, with a graphite crucible as a susceptor and a MgO crucible as the refractory container. The selected steel and slag compositions are shown in Tables 1 and 2, and Figure 1. A mass of 600 g of electrolytic iron and 0.66 g of iron(II)sulfide were melted and heated to 1600 °C, under a high-purity Ar atmosphere. Details of the experimental configuration were reported previously; previous experiments using the same configuration showed repeatability in characterizing steel–slag reaction kinetics and nonmetallic inclusion evolution [5,14–20]. From previous experiments, the concentration of dissolved oxygen in molten iron produced from the electrolytic iron is approximately 200 ppm (parts per million by mass). The molten iron was deoxidized using a laboratory-produced silicomanganese alloy (SiMn) with an approximate composition of 69%Mn-19%Si-10%Fe-2%C, added as 5–10 mm lumps. After deoxidation, 100 g of a pre-fused mixture of CaO, MgO, $Al_2O_3$, and $SiO_2$ (composition shown in Table 2 and Figure 1) was added to the top of the steel melt. The steel and slag were held for 3 h, during which time steel samples were taken using cylindrical fused-quartz sampling tubes (4 mm inside diameter).

After 3 h, the steel was intentionally reoxidized to precipitate out dissolved Mg and Ca as oxide inclusions. For reoxidation, 3 g of electrolytic iron was used; the electrolytic iron had been oxidized beforehand in the air at 800 °C, causing an increase in mass (oxygen pickup) of 0.02 g (measured with a 0.0001 g-resolution balance). An additional steel sample was taken after reoxidation.

**Table 1.** Aimed steel composition at deoxidation, for laboratory trial.

| | wt%C | wt%Si | wt%Mn | ppm $O_{tot}$ | ppm S |
|---|---|---|---|---|---|
| Aim | 0.03 | 0.33 | 1.15 | 200 | 400 |

**Table 2.** Aimed slag composition for laboratory trial.

| | wt%CaO | Wt%$SiO_2$ | Wt%MgO | Wt%$CaF_2$ |
|---|---|---|---|---|
| Aim | 56 | 24 | 5 | 15 |

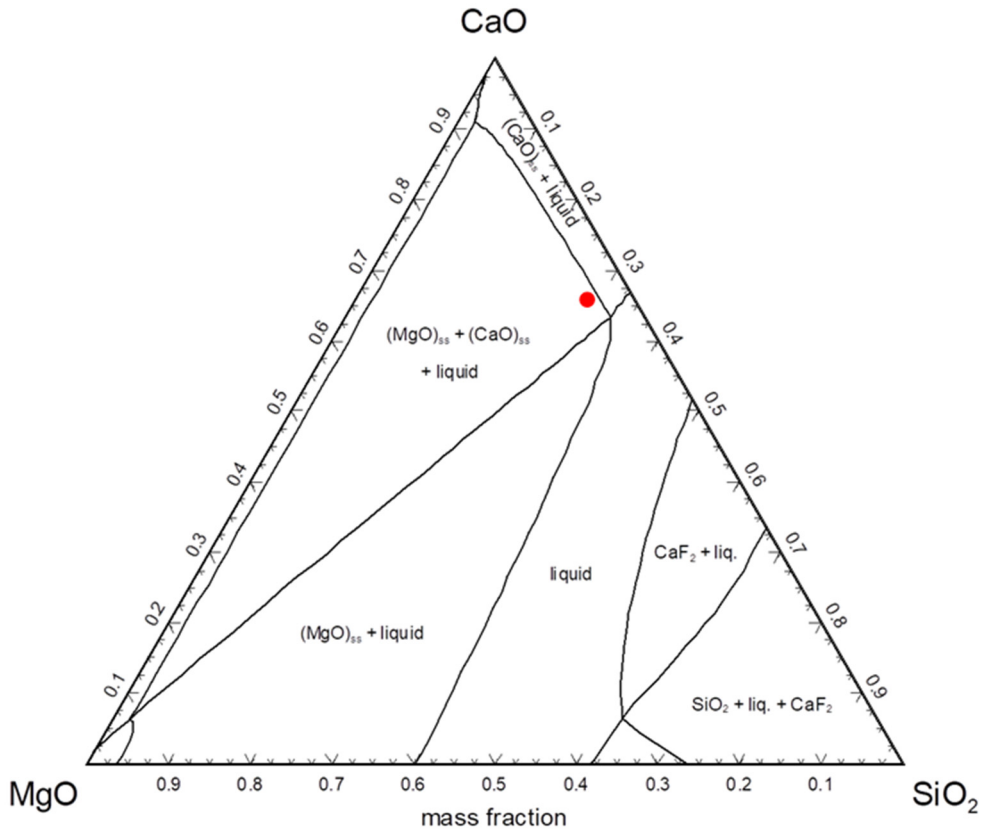


**Figure 1.** Pseudo-ternary CaO-$SiO_2$-MgO-15%$CaF_2$ phase diagram (isothermal section at 1600 °C) as plotted with FactSage 8.1 using the FToxid database (SLAGH liquid slag model). The red dot is the aimed composition to ensure double saturation with both $(MgO)_{ss}$ (periclase) and $(CaO)_{ss}$ (lime).

Cross sections of the steel samples were mounted and metallographically polished to a one-micron finish for nonmetallic inclusion analysis by scanning electron microscopy with energy-dispersive X-ray microanalysis (SEM/EDS). An FEI ASPEX Explorer instrument was used, at an accelerating voltage of 10 kV, an approximate spot size of 45%, and a magnification of 1200×. For these conditions, the spatial resolution was approximately 0.4 micron; the pixel size on scanning electron micrographs was 0.25 micron [21]. The samples were also chemically analyzed for bulk composition, by combustion analysis for [S] (performed at the US Steel Research Center), and ICP-MS for [Si], [Mn], and [Mg] (performed at R.J. Lee Group). The slag was analyzed via X-ray fluorescence (XRF), using an instrument manufactured by Bruker.

### *2.2. Modeling Setup*

A steel–slag–inclusion kinetic simulation was set up, using FactSage macro processing interfacing with Microsoft Excel to calculate the expected chemical interaction between the slag, deoxidized steel, and inclusions within the steel. The calculation procedure and assumptions were as described previously [14,22,23]. In these calculations, no fitting parameters are needed; only the mass transfer coefficient in the steel needs to be calibrated. This mass transfer coefficient was estimated from the analyzed [S] in the steel.

## 3. Results

### *3.1. Experimental Measurements*

The evolution over time of the steel composition, and the oxide inclusion composition and size are plotted in Figures 2–4. The sizes shown in Figure 5 are the apparent two-dimensional sizes (equivalent circle diameters). The [S] decayed from its initial value of 400 ppm to 4 ppm after 125 min (Figure 2). Over the same period, the [Si] levels dropped from

0.26% to 0.16%, and [Mn] from 1.34% to 1.18%. The final experimental slag composition is shown in Table 3.

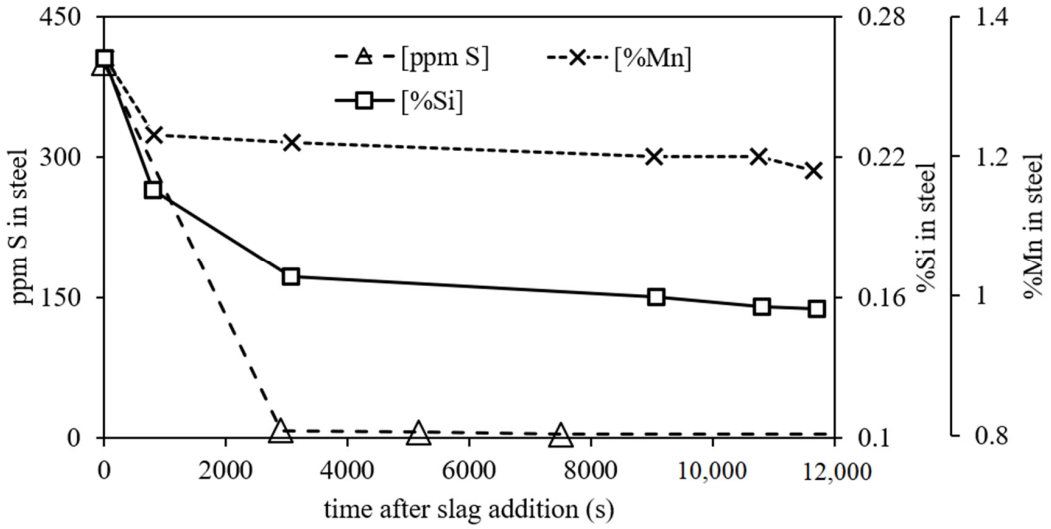


**Figure 2.** Evolution of chemical composition of steel in contact with basic slag over time after slag addition. Triangular markers represent the evolution of [S], × markers represent [Mn], and squares [Si].

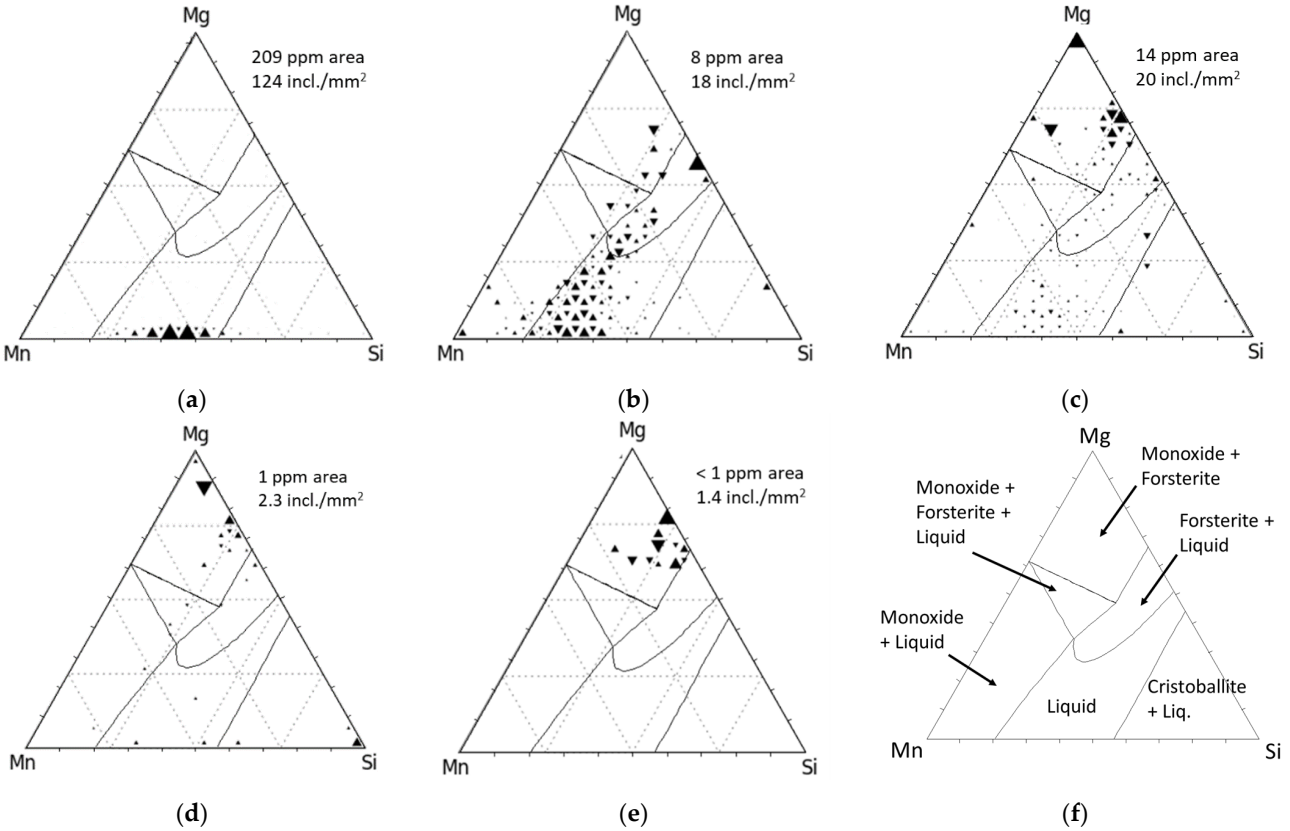


**Figure 3.** Ternary diagrams showing nonmetallic inclusion evolution during a steel–slag reaction. Inclusion compositions (as analyzed by SEM/EDS) are plotted as mole fractions of MnO, $SiO_2$, and MgO. Each ternary represents a sample taken at different times: (**a**) immediately before slag addition, and (**b**) 800 s, (**c**) 1580 s, (**d**) 3080 s, and (**e**) 4540 s after slag addition. The triangles are proportional to the area fraction of that nonmetallic inclusion composition. Ternary (**f**) is the isothermal section of MnO-$SiO_2$-MgO at 1600 °C (calculated using FactSage 8.0).

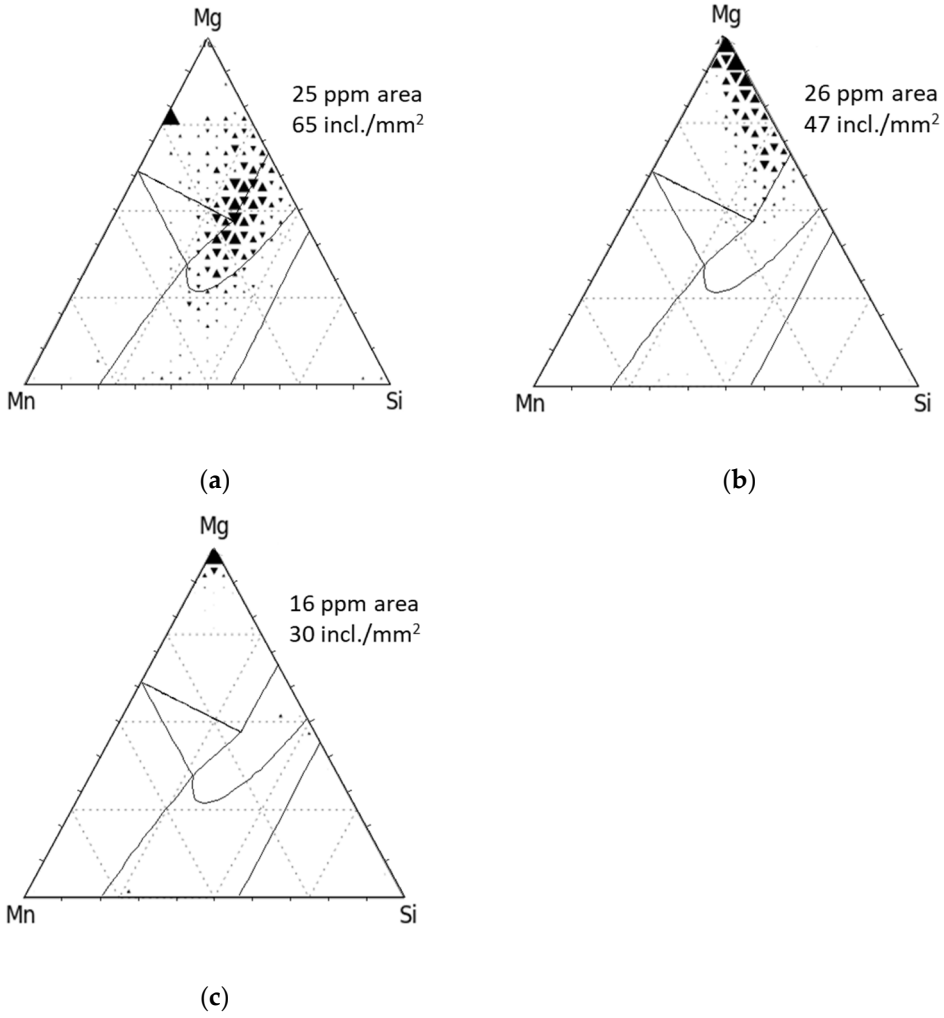


**Figure 4.** Inclusion compositions after intentional reoxidation of the steel, for samples taken (**a**) 10,820 s after slag addition, immediately after reoxidation; (**b**) 11,360 s after slag addition, 600 s after reoxidation; (**c**) 10,820 s after slag addition, 960 s after reoxidation.

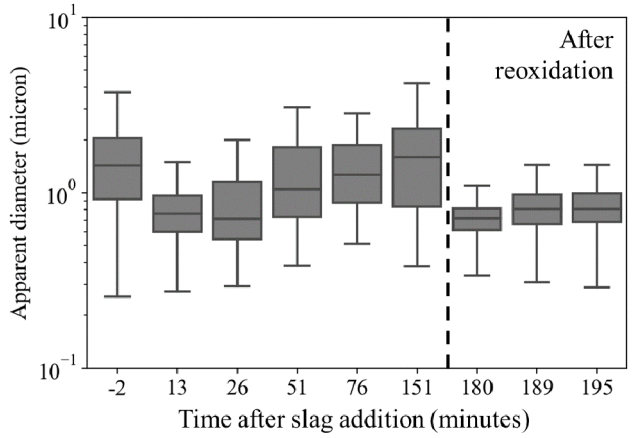


**Figure 5.** Box plots showing the evolution of size distribution of nonmetallic inclusions for each sample over time before slag addition, after slag addition, and after reoxidation with reoxidized electrolytic iron (the three samples after the dashed vertical line).

**Table 3.** XRF analysis results (as cation wt%) of oxide slag before and after the experiment.

| | wt%$Ca^{2+}$ | wt%$Si^{4+}$ | wt%$Mg^{2+}$ | wt%$Al^{3+}$ |
|---|---|---|---|---|
| Aim | 48 | 11 | 3 | 0 |
| Final | 51 | 8 | 2.5 | 0.4 |

From Figures 3 and 5, it can be seen that before slag addition, the nonmetallic inclusions were near-equimolar manganese silicates with sizes up to 4 μm. With the onset of the steel–slag reactions, it is seen that, after 13 min, the inclusions had transformed from manganese silicates into mixtures of liquid (Mn,Mg)-silicates and a forsterite-based solid solution [$(Mg,Mn)_2SiO_4$]. The steel became progressively cleaner with time, reducing from 50 ppm total oxygen (estimated from the total area fraction of inclusions) to less than 10 ppm within 15 min (as seen in Figure 3). During the remaining time before reoxidation of steel, the nonmetallic inclusion compositions remained in the monoxide–forsterite region, where the monoxide phase is the (Mg,Mn)O solid solution.

After reoxidation of the steel, there was an increase in the nonmetallic inclusion area fraction (from less than 1 ppm to 25 ppm) and in the estimated total oxygen in the steel (from less than 1 ppm to 6 ppm), indicating efficient transfer of O as iron oxides into the melt. Figure 5 shows that the reoxidation products were much smaller than the preexisting monoxide–forsterite inclusions, ranging from 0.3 micron diameter (close to the microscope resolution) to about 1 micron. The formation of fine nonmetallic inclusions indicates that the reaction mechanism is the dissolution of oxygen in the steel and subsequent reaction of deoxidants in steel with the dissolved oxygen [23]. The initial population of inclusions immediately after reoxidation consisted mostly of forsterite. After 10 min, the forsterite particles were partially converted into MgO and fully converted to MgO after 16 min.

The appearance of forsterite particles upon reoxidation indicates that at least 2.6 ppm of dissolved [Mg] was present in the steel at that time. Dissolved magnesium also remained in solution after this time or was replenished by Si-MgO reaction, causing the inclusion compositions to change over time as steel–slag–inclusion reactions approached equilibrium (since the slag was saturated with MgO, the equilibrium inclusion composition would be MgO).

The reoxidation inclusions did not contain Ca, confirming that the concentration of [Ca] in steel is much lower than for [Mg] for deoxidized steel in contact with slag that is saturated with both periclase and lime.

### *3.2. Modeling*

To model the steel–slag–inclusion reactions, the mass transfer coefficient for steel-slag reactions was estimated from the observed rate of desulfurization. The two fits shown in Figure 6 consider different equilibrium [S] values. The final [S] after the experiment was 4.1 ppm, whereas according to FactSage the equilibrium [S] would be 1.2 ppm. The value of 4.1 ppm from the experiment provided a better fit, and the corresponding rate constant was used to calculate the steel mass transfer coefficient for this system, assuming steel mass transfer limitation and that desulfurization followed first-order reaction kinetics [24,25].

In Figure 7, the bound Mg and O concentrations (as ppm) estimated from the nonmetallic inclusion analyses are plotted, together with the results from the kinetic model. The kinetic modeling was performed twice—with and without the Mg*O associate. In the FactSage steel solution model, the interaction between dissolved Mg and dissolved oxygen is quantified by assigning an equilibrium constant to the formation of the Mg*O associate. In this model, the dissolved forms of magnesium are Mg atoms and Mg*O associates. Recent results [18] indicate that the current Mg*O associate model overestimates the concentration of dissolved magnesium (by a factor of 2 or 3). In this modeling study, Ca*O associates were not considered, an approach that has been shown to improve agreement with experiments [6].

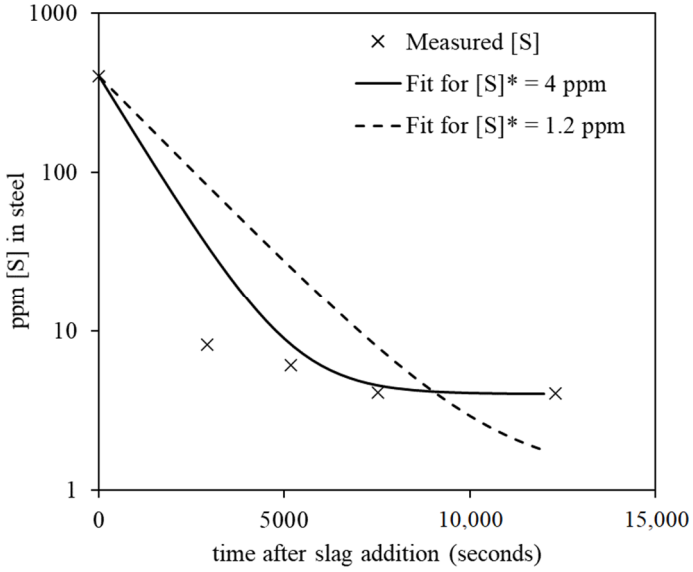


**Figure 6.** Measured evolution of [S] (markers) and fitted first-order reaction kinetics (lines) considering two equilibrium sulfur concentrations ([S]*): [S]* = 4 ppm (minimum [S] measured in the experimental trial; solid line), and [S]* = 1.2 ppm (FactSage estimate; broken line).

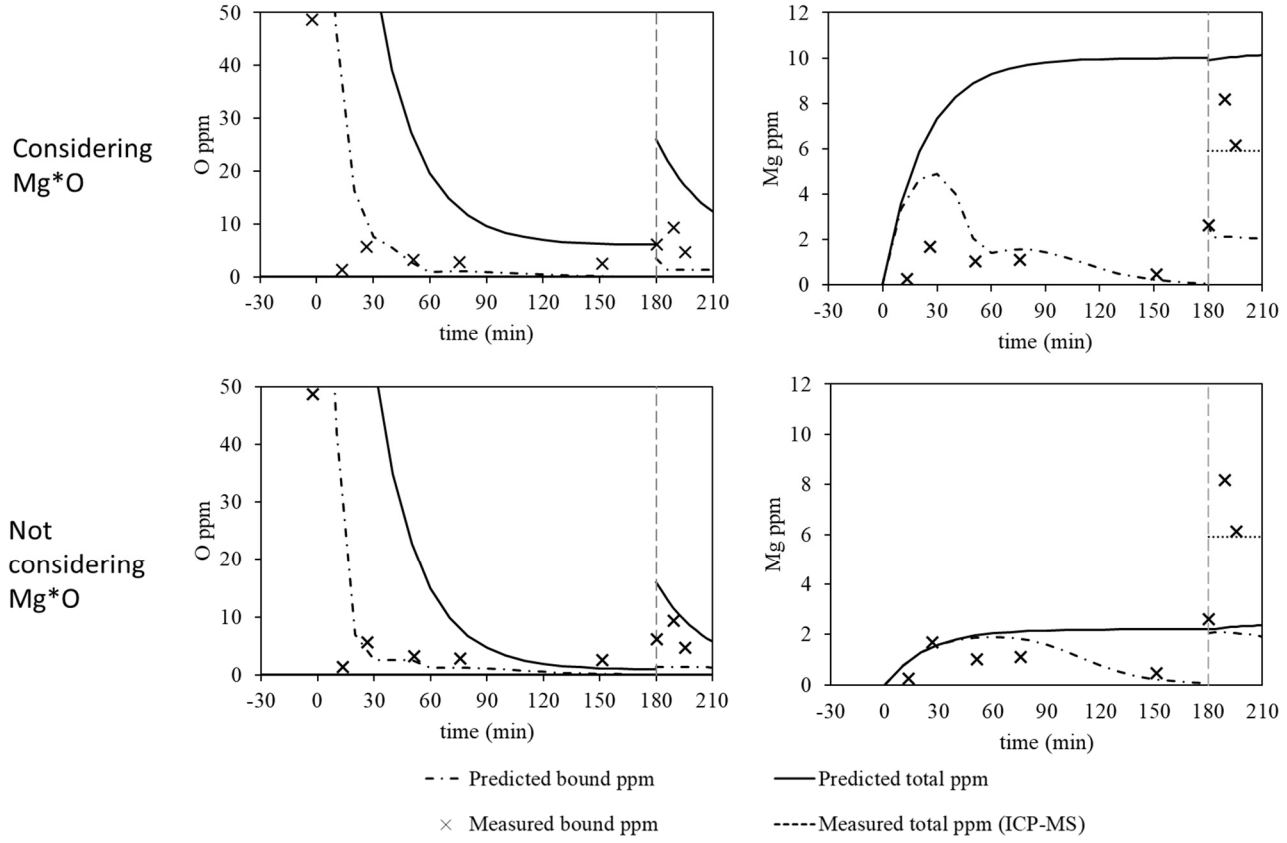


**Figure 7.** Comparison between the kinetic model predictions for total and bound magnesium and oxygen in the samples taken after slag addition and reoxidation, considering two different FactSage modeling scenarios: with the Mg*O associate model turned on, and off. The black, solid lines indicate the predicted total concentration of Mg and O, dot–dashed lines indicate the predicted concentrations of bound Mg and O, the × markers indicate the actual measurements based on the SEM/EDS analyses, and the horizontal dashed line indicate the final total Mg measured with ICP-MS. The time axis is relative to the moment of slag addition.

The main differences between the modeled Mg and O behavior, with and without Mg*O, are the following:

- The calculated equilibrium concentration of dissolved [Mg] is 10 ppm when Mg*O is considered, compared to the value of 2 ppm when Mg-O interaction is suppressed. For comparison, the analyzed total [Mg] in the steel after the experiments was 5.9 ppm in the sample taken 6 min after reoxidation. This total [Mg] includes both dissolved and bound forms of magnesium. From inclusion analysis, the average bound magnesium for the three samples taken after reoxidation was estimated as $6 \pm 3$ ppm (95% confidence interval). Immediately after reoxidation, the estimated bound magnesium concentration was 2.6 ppm.
- The predicted concentration of dissolved oxygen is higher if Mg*O is assumed to form.
- Agreement between the measured and predicted concentrations of bound Mg (before reoxidation) is better if the Mg*O associate is not considered.

## 4. Discussion

### *4.1. Desulfurization Reaction and Mn/Si Fade*

The overall desulfurization in this system can be described by Reaction (1).

$$2(\mathrm{CaO}) + [\mathrm{Si}] + 2[\mathrm{S}] = 2(\mathrm{CaS}) + (\mathrm{SiO_2}) \quad (1)$$

The measured final concentration of sulfur was slightly higher than predicted by FactSage, indicating an actual sulfur distribution coefficient of $L_S = (\%S)_{slag}/[\%S]_{steel} \approx 600$ rather than the FactSage prediction of $L_S \approx 2000$, closer to the results of Choi et al. [11] for similar steel and slag compositions ($L_S \approx 500$). The observed sulfur distribution coefficient is large, similar to that obtained for ladle desulfurization of Al-killed steel with calcium aluminate slag.

Given the stoichiometry of the desulfurization reaction, the observed [Si] consumption by deoxidation (removing ca. 200 ppm O) and desulfurization (removing 396 ppm S) would be 348 ppm. However, the total decrease in Si from the first to final steel samples was 1000 ppm. Similarly, between the first and second samples (taken before and after slag addition), a significant Mn and Si decrease (of 1100 ppm Mn and 560 ppm Si) was measured. The mass ratio between the decreases in total Si and Mn between the first and second samples, as seen in Figure 2, is 1.96. A possible mechanism for these decreases in Si and Mn concentration contains the following two elements: (1) the initial oxygen concentration in the molten iron could have been underestimated—both Mn and Si are consumed in forming the approximately equimolar MnO-$SiO_2$ deoxidation product; (2) the resulting deoxidation products are readily absorbed by slag and crucible (and therefore removed from the steel) [26,27]. This hypothesis is supported by the mass ratio of Mn/Si in the $MnSiO_3$ deoxidation product, which is 1.96 (54.94 g Mn/mol and 28 g Si/mol). Although this could explain the initial decrease in Mn, subsequent approach to equilibrium would involve the reduction of MnO by Si; no such recovery of the Mn concentration was observed. One possibility is that the reaction product is incorporated by the crucible, which can have a relatively slow reaction rate [5,27].

### *4.2. Effect of [Mg] Pickup into Nonmetallic Inclusion Composition Prior to Reoxidation*

Pickup of Mg by the liquid steel by reaction with the slag occurs by Reaction (2).

$$(\mathrm{MgO}) + [\mathrm{Si}] = [\mathrm{Mg}] + (\mathrm{SiO_2}) \quad (2)$$

According to FactSage, $a_{SiO_2(cristobalite)} = 6 \times 10^{-5}$ for the 56%CaO-24%$SiO_2$-3%MgO-15%$CaF_2$ slag at 1600 °C. The activity of $SiO_2$ is much higher in phases found in nonmetallic inclusions, such as $MnSiO_3$ ($a_{SiO_2} = 0.72$) and $Mg_2SiO_4$ ($a_{SiO_2} = 0.08$). This means that the concentration of [Mg] at the steel–slag interface would be much higher than at the steel–inclusion interfaces (for such inclusion compositions), even accounting for possible differences in MgO activity.

The mechanism for inclusion transformation is that [Mg] that is picked up by steel-slag reaction is transported into the steel; this [Mg] is then reoxidized by the oxide inclusions in the bulk of the steel, reducing MnO and $SiO_2$ out of the nonmetallic inclusions by Reactions (3) and (4).

$$(MnO) + [Mg] = (MgO) + [Mn] \quad (3)$$

$$(SiO_2) + 2[Mg] = 2(MgO) + [Si] \quad (4)$$

While the analyzed bound Mg content (in inclusions) rapidly increased to around 2 ppm, in parallel, there was a decrease in bound oxygen from 48 ppm to 6 ppm, as seen in Figure 7. This fade is related to inclusion flotation, as well as possible destabilization of oxide inclusions by slag deoxidation. Slag deoxidation involves the transport of dissolved oxygen to the steel–slag interface, decreasing the concentration of dissolved oxygen in the bulk steel. The resulting destabilization of Mn–silicates can be written as Reactions (5) and (6).

$$(MnO) = [Mn] + [O] \quad (5)$$

$$(SiO_2) = [Si] + 2[O] \quad (6)$$

In all cases, as time progresses, the reactions approach equilibrium, and the total concentration of inclusions tends to zero; thus, the bound Mg concentration also tends to zero.

### *4.3. Reoxidation and Nonmetallic Inclusions*

The introduction of oxygen (as a fragment of oxidized electrolytic iron) successfully reoxidized the steel, since the apparent bound [O] concentration rose from less than 1 ppm to 7 ppm O. However, this is much less than the oxygen addition: as noted earlier, the mass of added oxygen was approximately 20 mg, corresponding to a total oxygen addition of around 30 ppm. Reasons for the difference include (1) a significant concentration of dissolved oxygen (Figure 7) and (2) non-detection of small oxide inclusions (the reoxidation inclusions were just larger than the spatial resolution of the instrument).

The formation of forsterite and MgO inclusions indeed indicate that a significant amount of [Mg] had been dissolved in the steel at the onset of reoxidation. As shown by the inclusion analyses, reoxidation formed MgO, MnO, and $SiO_2$.

It is both predicted by FactSage and observed in the experiments that the [Mg] pickup from the slag continued after reoxidation since the change in [Si]—the reductant in Reaction (2)—was insignificant. Subsequent to reoxidation, [Mg], which was replenished by steel–slag reaction, reduced the reoxidation inclusions, forming MgO (Figure 4).

The estimated bound Mg concentration (based on inclusion analysis) for the three samples taken after reoxidation agrees with the ICP measurement for $Mg_{total}$ of 5.9 ppm in the sample taken 960 s after reoxidation (equivalent to Figure 4c). Given that little bound magnesium was detected in the sample taken immediately before reoxidation (Figure 7), the dissolved Mg concentration before reoxidation must have been at least 6 ppm. This concentration is higher than predicted without considering the Mg*O associate (2 ppm) but lower than with the associate (10 ppm). Overall, the Mg*O associate model used by FactSage better predicts the [Mg] solubility and transfer into steel; however, the excess oxygen expected from the Mg*O was not observed to reprecipitate upon cooling and solidification. According to Figure 7, there should be at least 5 ppm dissolved oxygen (as Mg*O) in samples taken right before reoxidation, but 1 ppm or less than 1 ppm area fraction of inclusions was detected in the samples represented in Figure 3d,e.

## 5. Conclusions

In this work, it was observed that deep desulfurization and deoxidation of Si-killed steel in contact with CaO-$SiO_2$-$CaF_2$-MgO slag was reproduced by laboratory experimentation. In parallel with desulfurization, [Si] also reduced MgO from the slag. The resulting [Mg] reacted with dissolved oxygen and manganese silicates to form (MgO). Over time, the

inclusions progressed from liquid manganese silicates to solid forsterite and MgO. Reoxidation of the steel reprecipitated dissolved [Mg] as smaller forsterite particles, which rapidly reverted to MgO. Since the mechanisms of desulfurization and [Mg] pickup are governed by the same kinetics and thermodynamics in full-sized ladles, the same mechanisms are expected to act on the industrial scale.

**Author Contributions:** Conceptualization, S.P.T.P. and P.C.P.; methodology, S.P.T.P.; software, S.P.T.P.; validation, S.P.T.P.; formal analysis, S.P.T.P.; investigation, S.P.T.P.; resources, P.C.P.; data curation, S.P.T.P.; writing—original draft preparation, S.P.T.P.; writing—review and editing, P.C.P.; visualization, S.P.T.P.; supervision, P.C.P.; project administration, P.C.P.; funding acquisition, P.C.P. All authors have read and agreed to the published version of the manuscript.

**Funding:** Support of this work by the industrial members of the Center for Iron and Steelmaking Research is gratefully acknowledged. We acknowledge the use of the Materials Characterization Facility at Carnegie Mellon University supported by Grant MCF-677785. Financial support of Stephano P. T. Piva by CAPES under the process BEX 13379/13-5–Doutorado Pleno/Ciência Sem Fronteiras is gratefully acknowledged.

**Institutional Review Board Statement:** Not applicable.

**Informed Consent Statement:** Not applicable.

**Data Availability Statement:** Datasets available to members of the Center for Iron and Steelmaking Research, upon request.

**Conflicts of Interest:** The authors declare no conflict of interest.

## References

1. Kaushik, P.; Lehmann, J.; Nadif, M. State of the art in control of inclusions, their characterization, and future requirements. *Metall. Mater. Trans. B* **2012**, *43*, 710–725. [CrossRef]
2. Allibert, M.; Gaye, H.; Geiseler, J.; Janke, D.; Keene, B.J.; Kirner, D.; Kowalski, M.; Lehmann, J.; Mills, K.C.; Neuschültz, D.; et al. *Slag Atlas*, 2nd ed.; Verlag Stahleisen GmbH: Düsseldorf, Germany, 1995; ISBN 3-514-00457-9.
3. Seo, W.-G.; Han, W.-H.; Kim, J.-S.; Pak, J.-J. Deoxidation Equilibria among Mg, Al and O in Liquid Iron in the Presence of MgO $Al_2O_3$ Spinel. *ISIJ Int.* **2003**, *43*, 201–208. [CrossRef]
4. Itoh, H.; Hino, M.; Ban-Ya, S. Thermodynamics on the formation of spinel nonmetallic inclusion in liquid steel. *Metall. Mater. Trans. B* **1997**, *28*, 953–956. [CrossRef]
5. Kumar, D.; Pistorius, P.C. Rate of MgO Pickup in Alumina Inclusions in Aluminum-Killed Steel. *Metall. Mater. Trans. B* **2019**, *50*, 181–191. [CrossRef]
6. Liu, C.; Kumar, D.; Webler, B.A.; Pistorius, P.C. Calcium Modification of Inclusions via Slag/Metal Reactions. *Metall. Mater. Trans. B* **2020**, *51*, 529–542. [CrossRef]
7. Kumar, D.; Piva, S.P.T.; Pistorius, P.C. Transfer of calcium to oxide inclusions in steel without calcium treatment. In Proceedings of the 10th International Conference on Clean Steel, Budapest, Hungary, 18–20 September 2018.
8. Verma, N.; Pistorius, P.C.; Fruehan, R.J.; Potter, M.; Lind, M.; Story, S. Transient inclusion evolution during modification of alumina inclusions by calcium in liquid steel: Part I background experimental techniques and analysis methods. *Metall. Mater. Trans. B* **2011**, *42*, 711–719. [CrossRef]
9. Harada, A.; Maruoka, N.; Shibata, H.; Kitamura, S. A Kinetic Model to Predict the Compositions of Metal, Slag and Inclusions during Ladle Refining: Part 1. Basic Concept and Application. *ISIJ Int.* **2013**, *53*, 2110–2117. [CrossRef]
10. Panda, D.; Ross, N.; McQuillis, G.; Jenkins, J. Method of Desulfurizing Steel. U.S. Patent 8,523,977 B2, 3 September 2013.
11. Choi, C.; Jo, S.; Kim, S.; Lee, K.; Kim, J. The Effect of $CaF_2$ on Thermodynamics of CaO-$CaF_2$-$SiO_2$ (-MgO) Slags. *Metall. Mater. Trans. B* **2004**, *35*, 115–120. [CrossRef]
12. Andersson, J.O.; Helander, T.; Höglund, L.; Shi, P.F.; Sundman, B. Thermo-Calc and DICTRA, Computational tools for materials science. *Calphad* **2002**, *26*, 273–312. [CrossRef]
13. Bale, C.W.; Bélisle, E.; Chartrand, P.; Decterov, S.A.; Eriksson, G.; Gheribi, A.E.; Hack, K.; Jung, I.H.; Kang, Y.B.; Melançon, J.; et al. FactSage thermochemical software and databases, 2010–2016. *Calphad Comput. Coupling Phase Diagr. Thermochem.* **2016**, *54*, 35–53. [CrossRef]
14. Piva, S.P.T.; Kumar, D.; Pistorius, P.C. Modeling manganese silicate inclusion composition changes during ladle treatment using FactSage macros. *Metall. Mater. Trans. B* **2017**, *48*, 37–45. [CrossRef]
15. Roy, D. Effect of Silicon on the Desulfurization of Al-killed Steels. Ph.D. Thesis, Carnegie Mellon University, Pittsburgh, PA, USA, 2012.
16. Ferreira, M.E. Inclusions Size Distributions After Calcium Treatment in Low Carbon Aluminum Killed Steels. Ph.D. Thesis, Carnegie Mellon University, Pittsburgh, PA, USA, 2018.

17. Mu, H.; Zhang, T.; Yang, L.; Xavier, R.R.; Fruehan, R.J.; Webler, B.A. In Situ Observation of MgO Inclusions in Liquid Iron-Aluminum Alloys. *Metall. Mater. Trans. B* **2016**, *47*, 3375–3383. [CrossRef]
18. Tang, D.; Pistorius, P.C. Non-metallic Inclusion Evolution in a Liquid Third-Generation Advanced High-Strength Steel in Contact with Double-Saturated Slag. *Metall. Mater. Trans. B* **2021**, *52*, 580–585. [CrossRef]
19. Manning, C.P.; Fruehan, R.J. The Rate of the Phosphorous Reaction Between Liquid Iron and Slag. *Metall. Mater. Trans. B* **2013**, *44*, 37–44. [CrossRef]
20. Piva, S.P.T.; Ferreira, M.E.; Kumar, D.; Pistorius, P.C. A Study on the Effect of Fluid Flow into Non-Metallic Inclusion Changes. In Proceedings of the 8th International Conference on Modeling and Simulation of Metallurgical Processes in Steelmaking (STEELSIM2019), Toronto, ON, Canada, 13–15 August 2019; AIST: Warrendale, PA, USA, 2019.
21. Tang, D.; Ferreira, M.E.; Pistorius, P.C. Automated Inclusion Microanalysis in Steel by Computer-Based Scanning Electron Microscopy: Accelerating Voltage, Backscattered Electron Image Quality, and Analysis Time. *Microsc. Microanal.* **2017**, *23*, 1082–1090. [CrossRef] [PubMed]
22. van Ende, M.A.; Jung, I.H. A Kinetic Ladle Furnace Process Simulation Model: Effective Equilibrium Reaction Zone Model Using FactSage Macro Processing. *Metall. Mater. Trans. B* **2017**, *48*, 28–36. [CrossRef]
23. van Ende, M.-A.; Guo, M.; Proost, J.; Blanpain, B.; Wollants, P. Formation and Morphology of $Al_2O_3$ Inclusions at the Onset of Liquid Fe Deoxidation by Al Addition. *ISIJ Int.* **2011**, *51*, 27–34. [CrossRef]
24. Turkdogan, E.T.; Fruehan, R.J. Fundamentals of Iron and Steelmaking. In *Making, Shaping and Treating of Steel: Steelmaking and Refining Volume*; The AISE Steel Foundation: Pittsburgh, PA, USA, 1999; Chapter 2; pp. 37–160.
25. Roy, D.; Pistorius, P.C.; Fruehan, R.J. Effect of silicon on the desulfurization of Al-killed steels: Part I. Mathematical model. *Metall. Mater. Trans. B* **2013**, *44*, 1086–1094. [CrossRef]
26. Ren, Y.; Liu, C.; Gao, X.; Zhang, L.; Ueda, S.; Kitamura, S. Dissolution Behavior of Mg and Ca from Dolomite Refractory into Al-killed Molten Steel. *ISIJ Int.* **2021**, *61*, 1–9. [CrossRef]
27. Piva, S.P.T.; Pistorius, P.C. Ferrosilicon-Based Calcium Treatment of Aluminum-Killed and Silicomanganese-Killed Steels. *Metall. Mater. Trans. B* **2020**, *52*, 6–16. [CrossRef]